Towards the Application of AI Technology to Assess Risk of Aneurysm Rupture Based on Medical Imaging

Relations of geometry, size, blood pressure, and wall strength

Fumio Nogata
Emeritus professor
Gifu University, Gifu, Japan
nogata [AT] gifu-u.ac.jp

Yasunai Yokota
Professor,
Faculty of Engineering
Gifu University, Gifu, Japan
ykt [AT] gifu-u.ac.jp

Yoko Kawamura
Faculty of Engineering
Gifu University, Gifu, Japan
yokokawa [AT] gifu-u.ac.jp

Tetsuya Mouri
Associate professor
Faculty of Engineering
Gifu University, Gifu, Japan
Mouri [AT] gifu-u.ac.jp

William R. Walsh
Professor
Prince of Wales Hospital
University of New South Wales
Kensington, Australia
w.walsh [AT] unsw.edu.au

Takahiko Kawamura
Chubu Rosai Hospital, Aichi, Japan
Diabetes and Endocrine Internal Medicine
kawamura.hsc [AT] chubuh.johas.go.jp

Nigishi Hotta
Emeritus professor of Nagoya University
Chubu Rosai Hospital, Internal Medicine
Aichi, Japan
hotta [AT] chubuh.johas.go.jp

Abstract—**The shape and size of aneurysms were quantified using an ellipsoidal equation and a new procedure was proposed to evaluate the mechanical stress associated with changes in the wall thickness due to aneurysm dilation and blood pressure. The aneurysm rupture risk (ARR) can be assessed quantitatively from stiffness and strength of the patient using changes in diameter of the common carotid artery (CCA) with ultrasonic imaging. APR can also be derived from the natural frequency of brachial artery wall oscillations or the external ear canal side of the superficial temporal artery (STA) with the pulsation. By using this method of digitizing the risk of aneurysm rupture and its related information, it is possible to save clinical data around the world as big data and obtain optimal diagnostic solutions by the application of statistics and probability based AI techniques. Therefore, hospitals around the world will always be able to obtain the highest level of objective diagnostic information, regardless of country or region.**

Keywords-computeter tomography; aneurysm ruputure; ellipsoid modeling; arteificial intelligench; in vivo sterength; ultrasonic imaging

I. INTRODUCTION

Aneurysms are known to occur in weakened areas of the blood vessel wall, a slight expansion of the aorta is called ectasia, and a bulge larger than 1.5 times the size of a normal artery is called an aneurysm [1-3]. An aneurysm may occur in any part of the body but is most common in the brain, thoracic aneurysm, abdominal aortic aneurysm (AAA), and legs of artery. The rupture of AAA represents a significant clinical event, having a mortality rate of 90% [4, 5], and e.g. in the case of AAA sizes greater than 50% of the normal artery diameter, approximately 15,000 people died a year in the United States [6,7]. The risk assessment of rupture, determining aneurysm examination and if surgery is required is to age related, smoking, hypertension, high blood pressure, size and growth rate over 5 years after diagnosis, and family history of aneurysm [8-13]. Recently, many guidelines have been issued by the European Society of Cardiology (ESC) as well as other societies and organizations [14]. This is a guideline for the purpose of giving the best final decision taking into consideration the effects of specific diagnostic or therapeutic measures and the risk-benefit ratio by patients, caregivers and responsible healthcare workers. However,

rupture of the aneurysm is caused by local tensile failure (true stress) of blood tissue in the vessel wall, but many guidelines use global parameters such as the shape of the aneurysm [15, 16], maximum diameter and growth rate [17-19]. Thus, it might not quantitatively reflect the actual risk for aneurysm rupture [20-23]. On the other hand, there are many reports that biomechanical considerations [20, 24-30] are one of the powerful tools to understand the actual rupture risk assessment and to predict its occurrence. In particular, the aneurysm shape model obtained from the XCT and MRI images was analyzed by finite element analysis (FEA). And then the wall stress criterion [22, 24], rupture potential index (RPI) [25, 26], and Peak Wall Rupture Risk Index (PWRI) [27, 28] etc. based on mechanical and mathematical consideration [29-30] have been proposed. As a global background in recent years, with the diversification of diet such as rapid aging, smoking and heavy alcohol use (lifestyle risks), the number of aneurysm patients abruptly increases and the examination image data gradually becoming huge amount. Therefore, it is urgent to establish a method for diagnosis based on biomechanical evaluation and introduction of artificial intelligence (AI) technology.

This paper presents a new biomechanical procedure to assess the risk of aneurysm rupture in preparation for the mathematical representation of aneurysm shape and size, and the application of AI techniques. Here, *in vivo* strength of the patient's arterial wall was evaluated using ultrasound imaging of the common carotid artery (CCA) [31] and/or the wall's natural frequency of artery [32]**.** And the rupture risk due to blood pressure and dilation of aneurysm will be mainly described. On the other hand, blood flow dynamics are thought to play an important role in the pathogenesis and treatment of cephalic aneurysms [33, 34], however, hemodynamic quantities of interest are difficult to measure in vivo. In this study, the problem of impaired blood flow to the inner wall of blood vessels, hemodynamic analysis not discussed.

II. SHAPE AND MECHANICS OF ANEURYSM

When the weakened portion of the vessel wall dilates, the vessel wall becomes thinner and blood pressure makes these mechanical stresses further greater. And because of the pulsation, the size of the aneurysm gradually increases with time. As a result, the wall ruptures when the stress due to blood pressure and the strength of the arterial wall of the patient become equal. Thus, in order to assess the risk of aneurysm rupture, the decrease in wall thickness and its stress as well as strength data are needed.

Figure 1 shows major tasks required to evaluate the risk of aneurysm rupture from the biomechanical viewpoint.

a) Shape and size: the evaluation of thickness reduction with aneurysm growth by applying computer-aided geometric identification with AI technology,

b) Stresses occurring in the aneurismal wall: the evaluation using mechanics equation for thin shell structures such as ellipsoidal body, and cylinder,

c) *In vivo* strength of artery with nondestructive measurement using ultrasonic image of the common carotid artery (CCA).

This report presents these tasks to assess the risk of aneurysm rupture towards the application of AI technology.

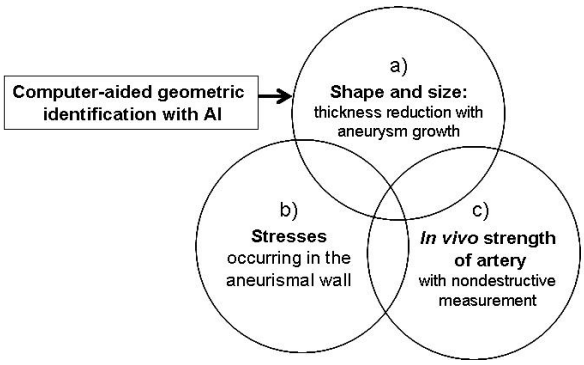

Figure 1. Major tasks required to assess the risk of aneurysm rupture from biomechanical viewpoint

A. Shape characterization and wall thickness reduction

Figure 2 shows some typical shapes of aneurysms, which are a) saccular-shaped (swelling only one side), b) fusiform-shaped (swelling all sides), c) berry-shaped on a narrow stem, and d) two-dimensional (2D) bulge of a tube due to blood pressure. Naturally, as the size of aneurysm increases, the arterial wall thickness decreases and mechanical stress rises, this acts to significantly increase the risk of rupture.

a) saccular aneurysm b) fusiform aneurysm c) berry aneurysm d) 2D bulge of tube

Figure 2. Typical shapes of aneurysms

When a cylindrical tube with a wall thickness t is expanded n times, the reduced thickness (t') is t/n in the case of the 2D cross section as shown in Fig. 3a). And a sphere (3D) is $1/n^2$ as in Fig. 3b). And an ellipsoidal body (3D) represented by the following equation:

$$x^2/a^2) + (\ y^2/b^2) + (\ z^2/c^2) = 1 \qquad (1)$$

This was dependent on the coefficients of a, b, and c as shown in Fig. 3c) and in Fig.4, and t' was about $1.06t//n^2$. Figure 4 shows the relationship between the expansion ratio (n) and the thickness's reduction ratio (t'/T) for three types of shapes shown in the Fig. 3. From this figure, it is note that the thinnest wall-thickness due to expansion of the aneurysm is sphere, thus the most likely to rupture. Therefore it could understand that if shape of aneurysm is characterized by the ellipsoidal equation, the risk of rupture can be evaluated easily the mechanical viewpoint of a shell structure. In the

case of the typical shape of the aneurysm shown in Fig. 2 which can be expressed in an ellipsoidal representation, a good curve fit of the wall of the blood vessel means a relatively soft arterial wall. On the other hand, the hardened blood vessels have a partially non-uniform shape, suggesting that the curve has a poor fit and a locally complicated stress occurs.

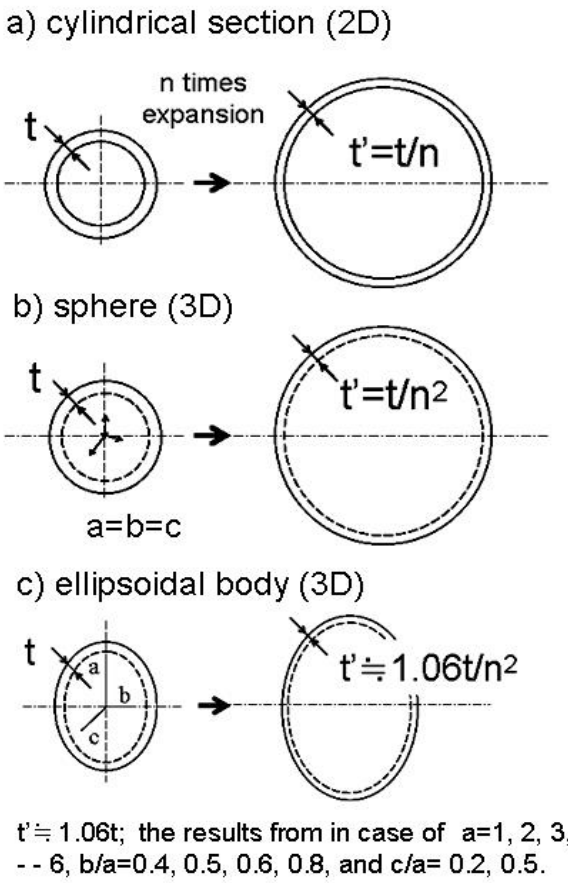

Figure 3. Contour shape of aneurysm and its thickness with expansion

Figure 5 shows the variation of ellipsoidal shape with a, b and c values. By changing these coefficients, it is possible to express various aneurysm shapes as well as reduction of thickness and their stress increasing. To summarize briefly, the risk of rupture of the aneurysm is not only the size, but it is very important to manage the expansion rate (the thickness) of the aneurysm as well as the mechanical stress against its time change. It is an effective way to formulate an aneurysm numerically for this purpose.

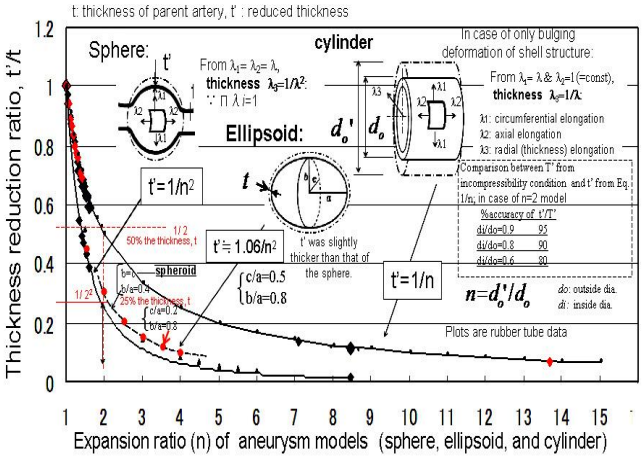

Figure 4. Relation between expansion ratio (n) and thickness reduction ratio (t '/ t) for several aneurysm models.

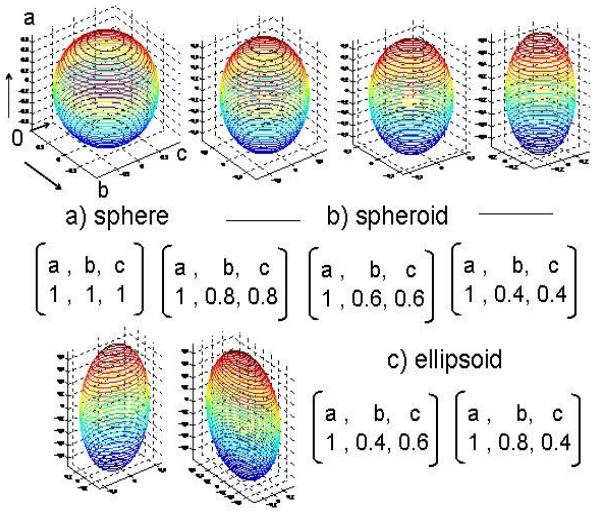

Figure 5. Variation of ellipsoidal shape with a, b and c values.The shape of the aneurysm is represented by finding these optimal coefficients.

B. Shape and its mechanical stresses

Figure 6 shows stress acting on a blood vessel wall due to blood pressure. There are two types of models, thin-walled and thick-walled cylindrical tube models from the mechanical viewpoint. A thin walled model is generally considered to be one whose walls are, thickness (t) /outer diameter (do) ratio, less than about 1/10 or 1/20 ($do/d \leq 1.25$ or $do/di \leq 1.11$, approximately). Blood vessels are two boundaries, but thin-walled cylindrical equations are simple equations, and the difference in stress value between them is small. In this report, we discussed as thick-walled model.

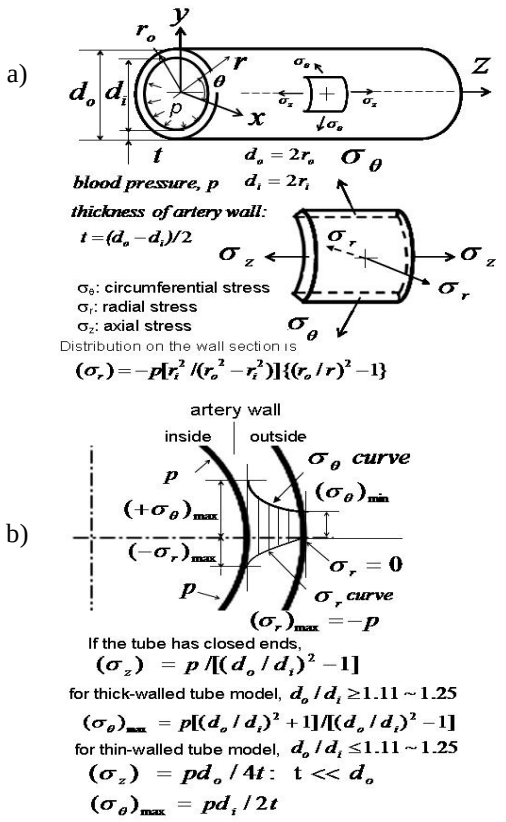

Figure 6. a) coordinate system of blood vessel: stresses acting on arterial wall by blood pressure, b) stress distribution of arterial wall (σ_θ and σ_r): the maximum stress is generated on the inner wall, ie a) coordinate system of blood vessel: stresses acting on arterial wall by blood pressure, b) stress distribution of arterial wall (σ_θ and σ_r): the maximum stress is generated on the inner wall, ie the crack starts from the inner wall.

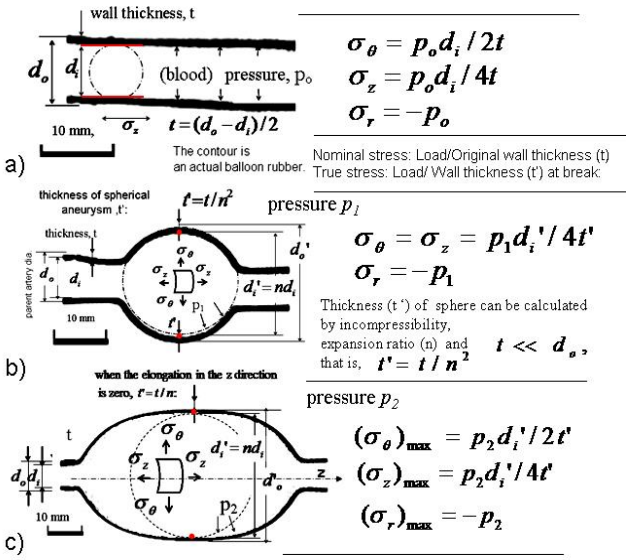

Recorded contour shape just before to rupture.

Figure 7. Contour shape of knob of balloon tube and its mechanical stresses.: a) tube at the internal pressrue p_o, b) spherical knob, c) fusiform-shape knob and true stress at p_2. The experimetal data (stress-strain curve) is shown in Fig. 10.

i) Rupture test of a rubber balloon as an artery model

The mechanical stress of the wall in the internal pressure rupture test is shown below using a rubber balloon tube (about Φ 6 mm).

Figure 7a) shows the original contour of a tube tested at the pressure p_o, 7b) is at the pressure p_1, and 7c) is at the pressure p_2, and then the tube that was ruptured at slightly larger pressure than at the p_2. These three contours show tube, sphere and fusiform-shaped whose the equation of mechanical stresses are shown in Fig. 7, respectively. Where t is the original wall thickness, t' is thickness at the p_o, thickness at p_1, thickness at p_2 and at the ruptured pressure ($p_2+\Delta p$). Note that nominal stress is determined from original thickness (t) before testing, and true stress is determined from the thickness (t') of the section at that pressured instant. And true stress is closely related to the true strength of the moment of aneurysm rupture. The experimental data including stress-strain curve are shown in the following section.

Rupture criterion: As mentioned above, the vessel wall is in a multi-axial stress state. In general, the equivalent tensile stress (von Mises stress) is used to predict failure criteria. This is mainly used for ductile materials and not for visco-elastic materials like arteries, but here the dilation of the aneurysm is a very slow phenomenon (a function of time is almost zero), so we used the Mises equivalent stress.

The von Mises stress is expressed as,

$$\sigma_{Mises} = \{[(\sigma_1 - \sigma_2)^2 + (\sigma_2 - \sigma_3)^2 + (\sigma_1 - \sigma_3)^2]/2\}^{1/2}, \quad (2)$$

and the failure criterion is

(maximum σ_{Misses}) $\geq$ (σ_{limit} of tensile strength of the patient).

Where the quantities of σ_1, σ_2, and σ_3 are three-dimensional principal stresses: $\sigma_1=\sigma_\theta$, $\sigma_2=\sigma_z$ and $\sigma_3=\sigma_r$. That is, if the von Mises stress is greater than the patient's tensile strength, the arterial wall breaks, , which means that the aneurysm ruptures.

ii) Stress equations of typical aneurysms

Figure 8a) is spherical saccular aneurysm which is the most common type of aneurysm. Assuming that the volume of the artery wall in the upper half of the parent artery (the neck portion diameter, dn) has swelled, the thickness due to expansion of this spherical aneurysm become $t'=(1/t^2)/2$.

Figure 8b) shows spherical berry aneurysm. Assuming that the volume of the wall in the parent artery (the neck portion diameter, dn) has swelled, the thickness due to expansion of this spherical aneurysm become $t'=(1/t^2)$. Then, true stress are given as $\sigma_\theta=\sigma_z=pd_d/2t'$ and $(\sigma_r)_{max}=-p$.

Figure 8c) shows ellipsoidal berry aneurysm.

When sphere shape (a=b=c),

$$\sigma_\theta=\sigma_z=pa/2t', \text{ and } (\sigma_r)_{max}=-p, \quad (3)$$

when spheroid shape (b=c), at the top T,

$$\sigma_\theta=\sigma_z=pa^2/2bt', \text{ and } (\sigma_r)_{max}=-p. \quad (4)$$

And at the equator, E,

$$\sigma_\theta=pat'\,[1-(1/2)(a^2/b^2)],\ \sigma_z=pa/2t' \text{ and } (\sigma_r)_{max}=-p. \quad (5)$$

It should be noted that if $(1/2)[a^2/b^2] > 1$, σ_θ will be negative (compressive stress) [35].

Figure 8d) shows saccular aneurysm which is asymmetrical and appear on one side of the aorta. These are usually caused by trauma or a severe aortic ulcer [1].

Figure 8e) is fusiform aneurysm which appears symmetrical bulges around the circumference of the aorta. They are the most common shape of aneurysm [1]. As mentioned above, these stresses in Figs. 8d) and 8e) are also applicable by the equations (3), (4), or (5) [35]. Therefore, rupture occurs at the point of the maximum Mises stress depending on the aneurysm shape (eg, point T). It is clear that the mathematical representation of the aneurysm shape can quantitatively represent the risk of rupture.

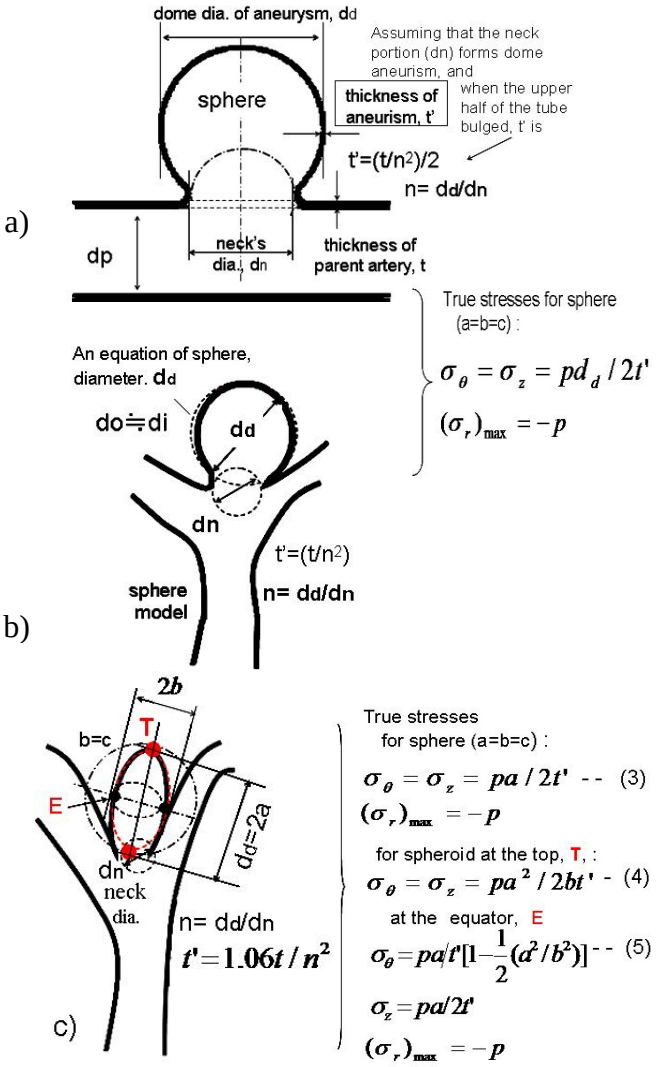

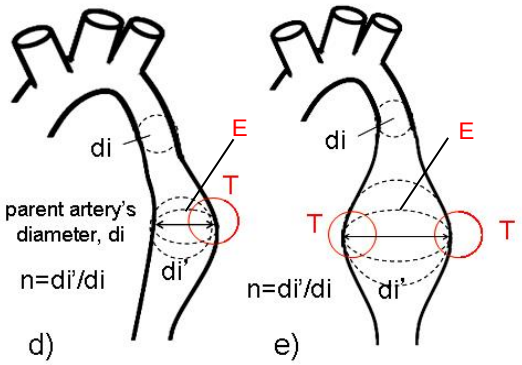

Figure 8. Typical aneurysms and their wall stresses : a) saccular-, b) and c) berry-, d) saccular-, and e) fusiform-aneurysm.

III. *IN VIVO* STRENGTH OF ARTERY

We describe two simple and inexpensive methods established for carotid and cranial artery strength in vivo [30, 31].

A. Definition of in vivo elastic stiffness (Eth) of artery

Arterial stiffening is the result of a decrease in elongation and strength from mechanical property point of view.

Figure 9 shows a schematic stress-strain relationship of arteries for both young and old adults, which shows a non-linear relationship due to the visco-elastic nature. Furthermore, the curve becomes steeper with age. Because of the time-dependent function, the mathematical expression that defines the stiffness of the artery is complex, so several equations have been proposed [4, 6-9].

In this report, the diameter variation of systolic blood pressure (Ps) at rest and diastolic blood pressure (Pd) is very small, for example, 3 to 16%, and thus we linearly defined between Ps and Pd . The hollow thick-walled cylinder model is as follows [31].

$$Eth=(BC/AC)=(\sigma_\theta/\varepsilon) \quad (6)$$

$$\sigma_\theta = [(d_o^2 + d_i^2)/(d_o^2 - d'^2)]\Delta p$$
$$\varepsilon = (\Delta d_i / d_i)$$

Where σ_θ and ε are hoop stress and strain respectively, di' means inner diameter at the Ps, and Δp=(Ps-Pd). And from the condition of no volume-change between Ps and Pd, the equation is

$$(d_o^2 - d_i^2) = (d'^2_o - d'^2_i). \quad (7)$$

From this definition, in vivo stiffness of the uniaxial tension test was Eth=0.53MPa, and internal pressure test was Eth=0.38MPa (see Fig. 11)); a slight difference was seen in this test piece.

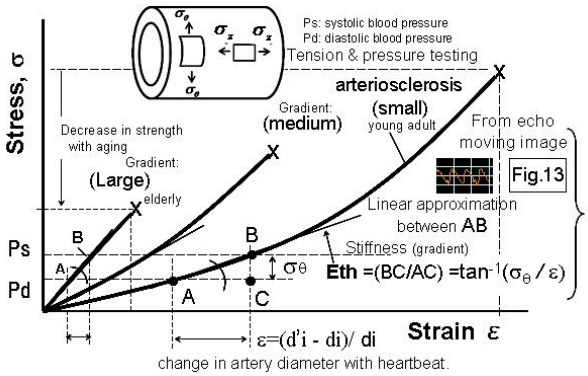

Figure 9. Stiffness (Eth) with arteriosclerosis and its definition.

B. Stress-strain relation of a rubber balloon

Figure 10 shows a typical curve of nominal stress and strain for a balloon tube (do=6.2, i= 5.4, t= 0.4mm). Two types of uniaxial tensile test specimens were used from the circumferential direction and the axial direction (longitudinal direction) of the tube. The internal pressure test is a test in which a stress nearly equal to that in the circumferential direction is applied. From the graph, it shows that the circumferential direction ((σ_θ)max=18.7MPa) was stronger than the axial direction ((σ_z)max=14.5MPa). On the other hand internal pressure test, bulge deformation is restrained due to triaxial-stress state, first, spherical bump occurred at the locally weakened portions of the rubber material, and then they became cylindrical bump and expanded in the axial direction (the diameter change was very small), then ruptured at nominal stress (σ_θ)max=2.25MPa (true stress were (σ_θ)max=(σ_1)=20.5MPa, (σ_z)max=(σ_2)=10.25MPa, (σ_r)max=(σ_3)=-p=35.5kPa from the Eqs. in Fig.7). The true stress value from the nominal stress was calculated from the maximum elongation at break or maximum bulge diameter the under constant volume conditions. To compare triaxial stress with uniaxial stress, the von Mises stress was $(\sigma_\theta)_{Mieses}$=18.4 MPa using equation (2), which is equivalent to the uniaxial tensile test result. Therefore, it was shown that the critical stress of internal pressure rupture is tensile failure stress.

C. Stress-strain relation of human artery

Figure 11 shows a typical curve of nominal stress and strain for the common carotid artery of the 80's (do=6.97, di= 5.31, t= 0.83mm). From the curve of uniaxial tension test, the nominal stress (σ_θ) max=0.54MPa) and the true stress were (σ_θ) max= (σ_1) **=0**.91MPa. And in the case of the pressrure test, nominal stress ((σ_θ)max=0.45MPa), true stress (σ_θ)max=(σ_1)=**0.**79MPa, also the von Mises stress$(\sigma_\theta)_{Mieses}$=0.69MPa were shown. Unlike the artificial material (balloon tube) test piece, there was a difference between two stress values; It may be due to partial hardening (sclerosis) of the specimen. From the viewpoint of in vivo arterial strength measurement, it was measured from the change in blood vessel diameter in rest. In addition, in vivo stiffness Eth were 0.63MPa (uniaxial test) and 0.38MPa (pressure test), respectively, showing in the Fig. 11.

D. A correlation between strength and stiffness:

Figure 12 shows the correlation between strength (tensile and burst pressure tests) and stiffness obtained from common carotid artery specimens of human (80's) and young sheep (24 months old). The correlation equation is given by

$$In\ vivo\ strength(MPa) = 7.0Eth^6 - 109.7Et^5 + 689.2Et^4 - 2234.5Eth^3 + 3951.8Eth^2 - 3727.9Eth + 1975.4 \quad (8)$$

Therefore, *in vivo* strength can be estimated from the change in blood vessel diameter at rest using the nondestructive measurement method described below. Furthermore, in order to make a graph with high correlation, it is necessary to add measurement data.

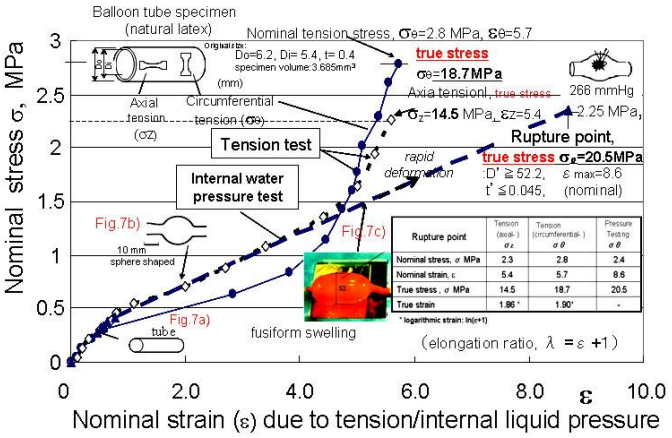

Figure 10. Stress-strain curve between nominal strain and stress of balloon tube (uniaxial tension and internal pressure test to rupture point).

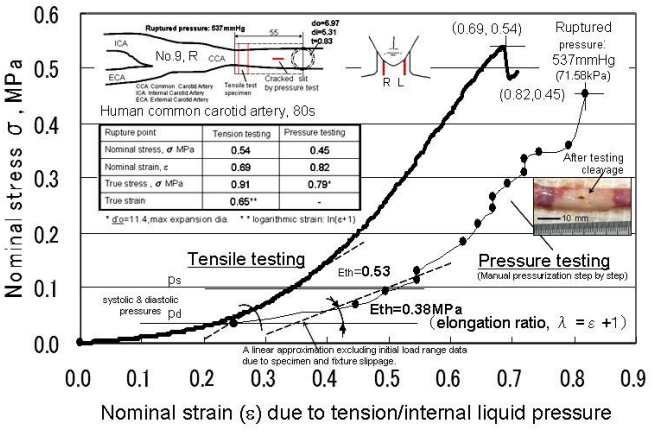

Figure 11. Stress-strain curve between tension and internal pressure tests (human common carotid artery, 80's)

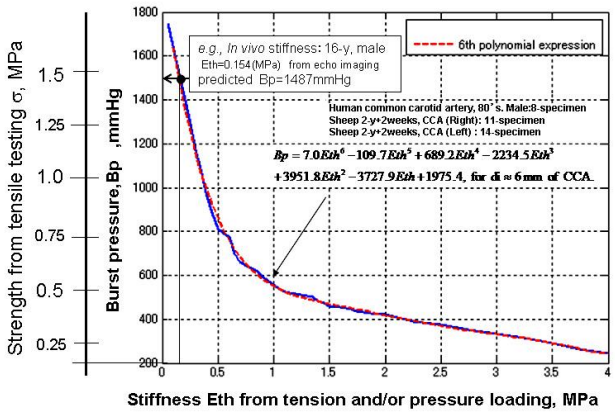

Figure 12. A correlation between stiffness (Eth) and burst pressure (Bp, experimentally ruptured) of the common carotid artery (CCA) for human and young sheep.

E. In vivo strength estimation with ultrasonic echo imaging

Figure 13 shows a system for estimating sclerosis of in vivo artery using ultrasonic B-mode image (540x420 pixel, 0.0713 mm/pixel linear probe). The variation of di is measured during several heartbeat times. And we assumed that do=di+wall thickness (t), (average t=~0.8mm; anatomical data for age of 40s~80s). We developed trial software [31] to estimate the variation of the di in real time.As a typical example, it was estimated in vivo Eth=0.154 MPa for young adult aged 16: in detail is shown in the figure. From Fig. 12 or Eq. (7), burst pressure is 1487mmHg which is about 12-time normal blood pressure. From the data for men aged 20 to 80 (159 men and 51 women on both sides of the CCA), the average burst pressure was 1000 mmHg for the aged 20, 800 mmHg for the age 40, 700mmHg for the age 60, and 550 mmHg for the age 80, which were in the case of health people[29]. However, because individual differences are large, it is important to measure blood vessel strength properly in the evaluation of aneurysm rupture.

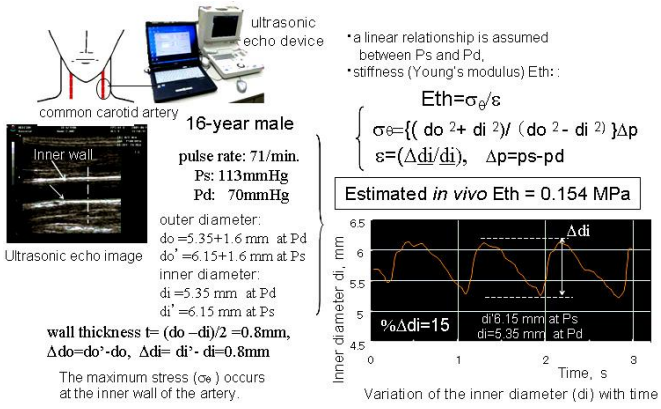

Figure 13. *In vivo* strength estimation with vibration analysis of artery wall. The system has developed for estimating strength of *in vivo* artery using B-mode ultrasound imaging[31]: the curve shows variation of di with time.

F. In vivo strength estimation with wall vibration analysis

We developed a new method [32] measuring arterial stiffness without using an ultrasonic device. The principle is the natural frequency of the vessel wall by the pulse wave. All structure has a natural frequency which is depend only on mass and stiffness of the system that is deformation resistance in response to an applied force. Therefore, stiffness of artery can be measured from the natural frequency of bulge vibration generated by variation of blood pressure.
The relationship between natural vibrations and stiffness for basic vibration systems can be found in the textbook.

Figure 14 shows a correlation between the natural frequencies measured (fn) on the skin surface and stiffness (Eth) of the CCA. Because of the influence of soft tissue around arteries, it was formulated as an experimental correlation.The following equation was obtained for the three arteries (upper extremity, superficial temporal artery and CCA).

$$Eth=0.014\,(fn) - 0.13, \quad R^2= 0.66. \tag{9}$$

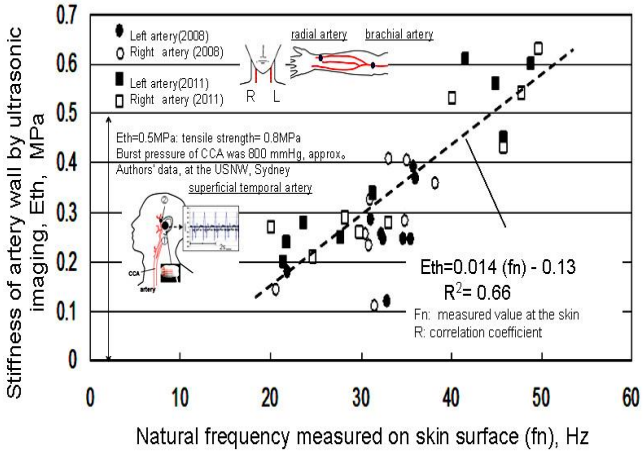

Figure 14. A correlation between the natural frequencies measured (fn) on the skin surface and stiffness (Eth) of CCA using ultrasonic imaging

Figure 15 shows the final procedures for assessing aneurysm rupture risk with the expansion ratio (n) for some typical aneurysms. These curves are calculated for two cases of blood pressures at 120 and 160 mmHg. Assumed that patient's CCA strength is 0.5 to 2.25MPa, it'll burst at n=2.6 times (120mmHg) or at n=2.25 times (160mmHg) of the parent artery size from the graphs. Unlike the current guidelines using the standard aneurysm size [14], the aneurysm expansion ratio (n) standard is our method. Therefore, the risk of aneurysm rupture can be assessed quantitatively from *in vivo* strength of the patient's, for example, the CCA.

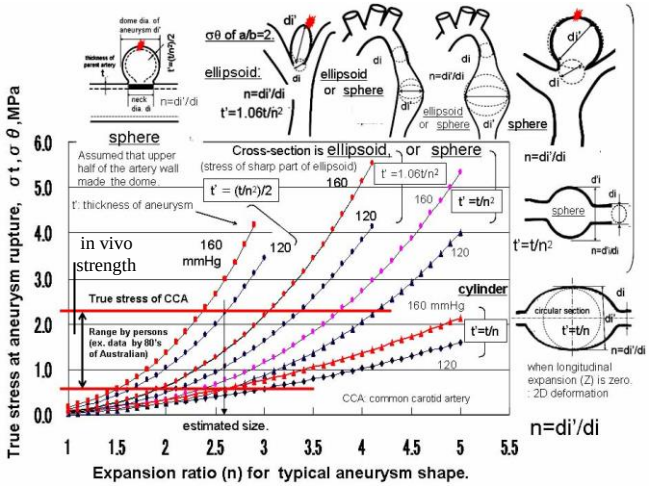

Figure 15. Relationship between rupture risk and expansion ratio (n) for some typical aneurysms: true stress is calculated using thickness (t '), and denominator of n is the parent artery size. The rupture risk can be assessed from the patient's arterial strength and n.

Figure 16 illustrates the procedures mentioned for formulating aneurysm shape and evaluating the risk of rupture. The risk of rupture can be assessed from aneurysm images and patient vessel strength data, enabling telemedicine diagnosis via the internet. This will lead to a technology that enables reasonable and appropriate medical examination that does not depend on hospital facilities, doctors and areas. Furthermore, to clarify the characteristics of the ruptured aortic aneurysm shape, it is feasible by big data analysis of the numerical value of the following items based on statistical probabilities.

1) Distribution of the coefficients (a, b, & c) in aneurysm at detection.
2) Distribution of the coefficients (a, b, & c) and wall thickness.

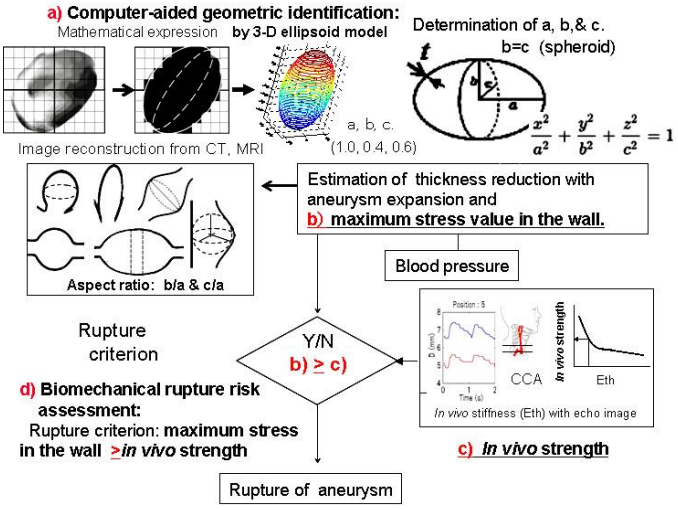

Figure 16. Procedure for assessing biomechanical aneurysm rupture risk from medical imaging.

3) Relation of the coefficients (a, b, & c), pre-ruptured wall stress, age, and gender.
4) Probability distribution of the coefficients (a, b, & c) just before rupture, and so on..

G. Towards application of AI technology for evaluation of rupture risk

Currently, aneurysm rupture risk diagnosis depends on hospital equipment, clinicians' experience and skills, area and country. We think that the same diagnosis must be made for the same disease. To realize, 1) the same specification equipment and the same examination procedures, 2)internet environment, 3) digitization of information, clinical data accumulation, statistic probability theory, machine diagnosis by AI technology application by deep learning etc., 4) Final diagnosis by world-class expert group on AI results, 5) obtaining the final diagnosis results from the cloud computing (international network), and 6) standard medical treatment procedures are need to be established. This will enable medical institutions around the world to receive community-independent treatment and care.

Figure 17 shows the procedures, which are global unified-optimal diagnosis by application of AI technology with cloud computing. We expect that by taking time and accumulating clinical data on diagnostic treatments around the world, this concept will establish as a more accurate method.

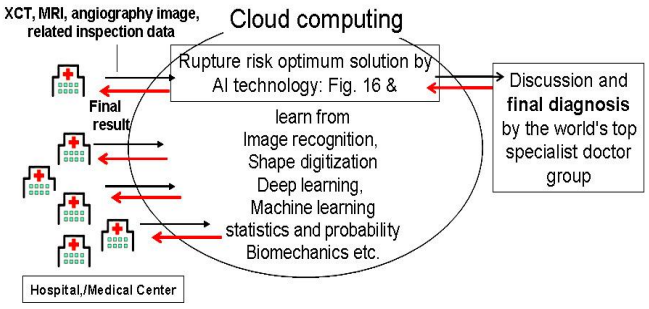

Figure 17. A global unified-optimal diagnosis by application of AI technology with cloud computing. This will help promote one diagnostic solution that is country, region, and hospital/medical center independent.

IV. CONCLUDING REMARKS

The current diagnostic procedures based on guidelines use aneurysm shape, maximum diameter and growth rate etc. Therefore, it may not reflect the actual rupture correctly. We believe that the establishment of diagnosis based on biomechanical evaluation and the introduction of artificial intelligence (AI) technology are considered to be the next issues. It is summarized as follows.

1) By expressing the aneurysm with an ellipsoidal equation, the reduction in wall thickness and stress related to rupture can be easily evaluated.
In case of the correlation between the shape and the mathematical expression is not good, it implies that there is a

local difference in the hardness of the blood vessel wall. In this case, simulation analysis by FEA etc. and management of rupture risk are recommended.

2) To measure in vivo blood vessel strength, techniques of ultrasonic and blood vessel vibration can be applied

3) By digitization of the aneurysm shape facilitates the application of AI techniques by mathematical processing in rupture risk management. Therefore, it enables reasonable and appropriate diagnosis independent of hospital equipment, doctors and areas. And the world's top level diagnostic will be available via the Internet.

ACKNOWLEDGMENTS

The authors express appreciation to all students and organizations cooperated in research from 2007 to 2012. The clinical investigations were performed according to the rules of the Ethics Committees of Gifu University Hospital and other participating hospitals.The work was partially supported by the Chiteki-Cluster Project (Gifu-Ohgaki Area) of the Ministry of Education, Science, Sports, and Culture of Japan.

REFERENCES

[1] University of Wisconsin Hospitals and Clinics, Heart, Vascular and Thoracic Care, https://www.uwhealth.org/heart-cardiovascular/types-of-aortic-aneurysms/10973

[2] Johnston KW, Rutherford RB, Tilson MD, Shah DM, Hollier L, Stanley JC, Suggested standards for reporting on arterial aneurysms. Subcommittee on Reporting Standards for Arterial Aneurysms, Ad Hoc Committee on Reporting Standards, Society for Vascular Surgery and North American Chapter, Inter.Soc. Cardiovascular Surg., J Vasc Surg., 1991;13(3),pp.452-458.

[3] Chaikof EL, Brewster DC, Dalman RL, Makaroun MS, Illig KA, Sicard GA, Timaran CH, Upchurch GR Jr, Veith FJ, The care of patients with an abdominal aortic aneurysm: the Society for Vascular Surgery practice guidelines., J Vasc Surg. 2009, 50(4 Suppl):S2.

[4] David A. Vorp, Jonathan P. Vande Geest, Biomechanical Determinants of Abdominal Aortic Aneurysm Rupture, *Arterioscler Thromb Vasc Biol*. August 2005, 2005;25:pp.1558-1566, & The online version of this article, along with updated information and services, on the http://atvb.ahajournals.org/content/25/8/1558.

[5] Patel MI, Hardman DT, Fisher CM, Appleberg M. Current views on the pathogenesis of abdominal aortic aneurysms. J Am Coll Surg. 1995, 181, pp.371-382.

[6] Sakalihasan N, Limet R, Defawe OD. Abdominal aortic aneurysm. *Lancet*. 2005;365,pp.1577-1589.

[7] Health Quality Ontario Endovascular repair of abdominal aortic aneurysm: an evidence-based analysis, Ontario Health Technol Assess Ser. 2002;2(1):pp.1-46.

[8] MJ, Thompson SG, Brown LC, Powell JT. Meta-analysis of individual patient data to examine factors affecting growth and rupture of small abdominal aortic aneurysms. Br J Surg 2012; 99, pp.655-665.

[9] Rughani G, Robertson L, Clarke M. Medical treatment for small abdominal aortic aneurysms. Cochrane Database Syst Rev 2012;9: CD009536.

[10] Ernst CB., Abdominal aortic aneurysm, The New England Journal of Medicine, (NEJM) 1993;328,pp.1167-1172.

[11] Cosford PA, Leng GC. Screening for abdominal aortic aneurysm. Cochrane Database of Systematic Reviews. 2007;2,CD002945. DOI: 10.1002/14651858.CD002945.pub2).

[12] Larsson E, Granath F, Swedenborg J, Hultgren R, A population-based case-control study of the familial risk of abdominal aortic aneurysm, J Vasc Surg. 2009 Jan; 49(1),pp.47-50.

[13] Brown PM, Zelt DT, Sobolev BG, The risk of rupture in untreated aneurysms: the impact of size, gender, and expansion rate. J Vasc Surg. 2003,37(2),pp.280-284.

[14] 2014 ESC Guidelines on the diagnosis and treatment of aortic diseases, European Heart Journal, doi:10.1093/eurheartj/ehu281,website (http://www.escardio.org/guidelinessurveys/escguidelines/about/Pages/rules-writing, aspx).

[15] Vorp DA, Raghavan ML, Webster MW, Mechanical wall stress in abdominal aortic aneurysm: influence of diameter and asymmetry., J Vasc Surg. 1998, 27(4):632-9.

[16] Hua J, Mower WR, Simple geometric characteristics fail to reliably predict abdominal aortic aneurysm wall stresses. J Vasc Surg. 2001 Aug; 34(2):308-15.

[17] Luciana Parlea, Rebecca Fahrig, David W. Holdsworth, and Stephen P. Lownie, An Analysis of the Geometry of Saccular Intracranial Aneurysms, AJNR Am J Neuroradiol,1999, 20,pp.1079-1089.

[18] Gasser TC, Nchimi A, Swedenborg J, Roy J, Sakalihasan N, Böckler D, Hyhlik-Dürr A., A novel strategy to translate the biomechanical rupture risk of abdominal aortic aneurysms to their equivalent diameter risk: method and retrospective validation., Eur J Vasc Endovasc Surg. 2014, 47(3):288-95.Stenbaek J, Kalin B, Swedenborg J., Growth of thrombus may be a better predictor of rupture than diameter in patients with abdominal aortic aneurysms., Eur J Vasc Endovasc Surg. 2000, 20(5):466-9.

[19] T. Christian Gasser, Biomechanical Rupture Risk Assessment , A Consistent and Objective Decision-Making Tool for Abdominal Aortic Aneurysm Patients, Aorta (Stamford). 2016 4(2), pp.42–60.

[20] Jeffrey Jim, Robert W Thompson, Clinical features and diagnosis of abdominal aortic aneurysm, https://www.uptodate.com/contents/clinical-features-and-diagnosis-of-abdominal-aortic-aneurysm, #H1382371318.)

[21] Janelle M. Guirguis-Blake, Tracy L. Beil, Xin Sun, Caitlyn A. Senger, MPH, Evelyn P. Whitlock, *Evidence Synthesis*, Number 109 Primary Care Screening for Abdominal Aortic Aneurysm: A Systematic Evidence Review for the U.S. Preventive Services Task Force, [Internet]. Agency for Healthcare Research and Quality (US); 2014 Jan.

[22] Maier A[1], Gee MW, Reeps C, Pongratz J, Eckstein HH, Wall WA.(A comparison of diameter, wall stress, and rupture potential index for abdominal aortic aneurysm rupture risk prediction, Ann Biomed Eng. 2010,38(10), pp.3124-3134.

[23] Wall stress 8. Fillinger MF, Raghavan ML, Marra SP, Cronenwett JL, Kennedy FE. In vivo analysis of mechanical wall stress and abdominal aortic aneurysm rupture risk. J Vasc Surg. 2002,36, pp.589 -597.

[24] A. Vorp, Jonathan P. Vande Geest, Biomechanical Determinants of Abdominal Aortic Aneurysm Rupture, Arterioscler Thromb Vasc Biol. is available at http://www.atvbaha.org, 2005, pp.1558-1566.

[25] Vande Geest JP, Di Martino ES, Bohra A, Makaroun MS, Vorp DA., A biomechanics-based rupture potential index for abdominal aortic aneurysm risk assessment. Ann NY Acad Sci. 2006,1085, pp.11-21.

[26] Doyle BJ, Callanan A, Walsh MT, Grace PA, McGloughlin TM. A finite element analysis rupture index (FEARI) as an additional tool for abdominal aortic aneurysm rupture prediction. *Vasc Dis Prev*. 2009,6,pp.114-121.

[27] Erhart P, Hyhlik-Dürr A, Geisbüsch P, Kotelis D, Müller-Eschner M, Gasser TC, von Tengg-Kobligk H, Böckler D.,Finite element analysis in asymptomatic, symptomatic, and ruptured abdominal aortic aneurysms: in search of new rupture risk predictors. Eur J Vasc Endovasc Surg. 2015, 49(3), pp.239-245.

[28] Watton P, Hill N, Heil M. A mathematical model for the growth of the abdominal aortic aneurysm. Biomechan Model Mechanobiol. 2004,3,pp.98–113.

[29] Volokh KY, Vorp DA. A model of growth and rupture of abdominal aortic aneurysm. J Biomech. 2008,41, pp.1015-1021.

[30] T. Christian Gasser,, Biomechanical Rupture Risk Assessment, A Consistent and Objective Decision-Making Tool for Abdominal Aortic Aneurysm Patients, AORTA, April 2016, Volume 4, Issue 2, pp.42-60
http://dx.doi.org/10.12945/j.aorta.2015.15.030, pp.42-60.

[31] F. Nogata, Yasunari Yokota; Yoko Kawamura, W.R Walsh, H. Morita, Y. Uno T. Kawamura[6], M. Nagashim[6], and N. Hotta, A Technique for Estimating Sclerosis of Carotid Artery with Ultrasonic Echo, European Conf. of the Inter. Federation for Medical and Eng., IFMBE Proc., WC2009, 25/IV,2009, pp.655-658.

F.Nogata, Y.Yokota, Y.Kawamura, H.Morita and Y. Uno, "Estimating of mechanical strength of in vivo common carotid artery using ultrasound echo images" Proc. ISBPE/The 22nd SICE Symposium. Harbin, China, 2007,pp.249-252.

F. Nogata, Y. Yokota; Y.Kawamura, W, R.. Walsh, T. Goto, ,K. Kagechika, Stiffness Estimation from Arterial Wall Vibration and its Application: new earphone for examining arteriosclerosis between music and next music, Inter. J. Computer and Infor. Tech. (ISSN: 2279 – 0764), Vol.06-01, 2017, pp.7-13.

[32] F. Nogata, Y. Yokota; Y.Kawamura, W, R.. Walsh, T. Goto, ,K. Kagechika, Stiffness Estimation from Arterial Wall Vibration and its Application: new earphone for examining arteriosclerosis between music and next music, Inter. J. Computer and Infor. Tech. (ISSN: 2279 – 0764), Vol.06-01, 2017, pp.7-13.

[33] for example, Sugiyama S[1], Meng H, Funamoto K, Inoue T, Fujimura M, Nakayama T, Omodaka S, Shimizu H, Takahashi A, Tominaga T., Hemodynamic analysis of growing intracranial aneurysms arising from a posterior inferior cerebellar artery, World Neurosurg., 2012,78(5),pp.462-468.

[34] for example, Metcalfe RW., The promise of computational fluid dynamics as a tool for delineating therapeutic options in the treatment of aneurysms., Am J Neuroradiol. 2003 Apr;24(4),pp.553-554

[35] R. K. Sinnot, Chemical Engineering Design, Chemical Engineering, Volume 6, Fourth edition, Elsevier, pp.798-804.